

# Output coupling from x-ray free-electron laser cavities with intracavity beam splitters

Yuri Shvyd'ko<sup>1,\*</sup>

<sup>1</sup>*Advanced Photon Source, Argonne National Laboratory, Argonne, Illinois 60439, USA*  
(Dated: November 13, 2021)

Permeable mirrors are typically used for coupling photons out of laser cavities. A similar approach was proposed for output coupling photons from the cavities of x-ray free-electron laser (XFEL) oscillators. One of the Bragg-reflecting crystal mirrors is thin, just a few extinction length, and is used as a permeable mirror. However, this method is very often limited to extractions of only a few tenths of the intracavity power. Other cavity-based XFELs, such as the high-gain regenerative amplifier XFEL, require much higher outcoupling efficiency. Here, alternative schemes are proposed and analyzed for coupling x-ray photons out of XFEL cavities using intracavity Bragg-reflecting, x-ray-transparent diamond crystal beam splitters. The intracavity beam splitters are efficient and flexible in terms of the amount of the power they are capable of coupling out of the cavity, an amount that can be varied promptly from zero to close to 100%. The schemes can be readily extended to multi-beam outcoupling.

PACS numbers: 41.50.+h, 41.60.Cr, 61.05.cp, 42.55.Vc

## I. INTRODUCTION

The next generation of high-repetition-rate x-ray free-electron lasers (XFELs) will allow for optical cavity feedback, like in classical lasers. Unlike self-amplified spontaneous emission (SASE) XFELs [1–3], cavity-based XFELs [4, 5] are capable of generating fully coherent x-ray beams of high brilliance and stability. Two major optical cavity-based XFEL schemes are presently under discussion: low-gain and high-gain.

An x-ray free-electron laser oscillator (XFEL) [5–7] is a low-gain cavity-based XFEL, which requires a low-loss (high-Q) cavity. XFELs are promising to generate radiation of unprecedented spectral purity (a few-meV bandwidths). Figure 1(a) shows an example schematic of the XFEL with a tunable cavity composed of four Bragg-reflecting flat-crystal “mirrors” (A, B, C, and D) and compound refractive lenses (CRLs) as collimating and focusing elements [6]. Alternative cavity designs can be considered as well, such as a tunable compact non-coplanar six-crystal cavity [8] or others. X-rays generated by electrons in the undulator circulate in the low-loss optical cavity composed of flat Bragg-reflecting diamond crystals with close to 100% reflectivity [9] and low-absorbing Be paraboloidal lenses [10, 11] stabilizing the cavity.

Because XFELs are low-gain devices, the outcoupling efficiency is typically required to be a few percent. A standard procedure for outcoupling in laser physics by using a partially reflective mirror can be extended to a hard x-ray regime, as well. Indeed, a similar approach was proposed for coupling photons out of the XFEL optical cavities [5, 6, 8] by using thin, permeable crystal mirrors.

Another possible realization of the cavity-based XFEL is a high-gain regenerative amplifier FEL (XRAFEL). It

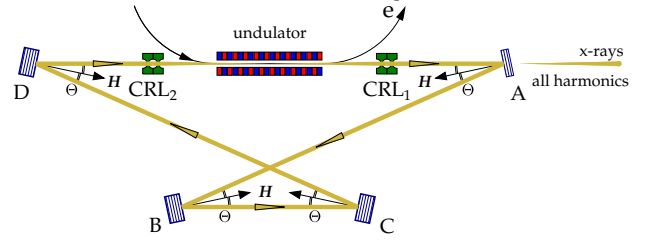


FIG. 1: Schematic of a cavity-based XFEL with a tunable optical cavity composed of four Bragg-reflecting flat-crystal mirrors (A, B, C, and D) and compound refractive lenses (CRLs) as focusing elements [6]. X-ray power is coupled out of the cavity through permeable thin crystal A with reduced reflectivity. The incidence and reflection angles  $\Theta = \pi/2 - \theta$  are the same for all crystals, where  $\theta$  is Bragg’s angle.

was first demonstrated in the infrared [12] and is also considered in the hard x-ray regime [4, 13, 14]. The XRAFEL optical cavity can be either the same tunable four-crystal cavity shown in Fig. 1, or a six-crystal cavity [8], or any alternative one. The XRAFEL is a high-gain FEL, which can reach saturation after a few round-trip passes. It can therefore allow for a high (close to 100%) extraction efficiency.

How can this be achieved? Can the permeable thin-crystal approach be extended to high-efficiency outcoupling required for XRAFEL? Are there other options? High-efficient output coupling using Bragg-reflecting pinhole crystal mirrors was proposed and studied in [14]. Here an alternative possibility is discussed, using intracavity, Bragg-reflecting, x-ray-transparent diamond crystal beam splitters.

\*Electronic address: shvydtko@aps.anl.gov

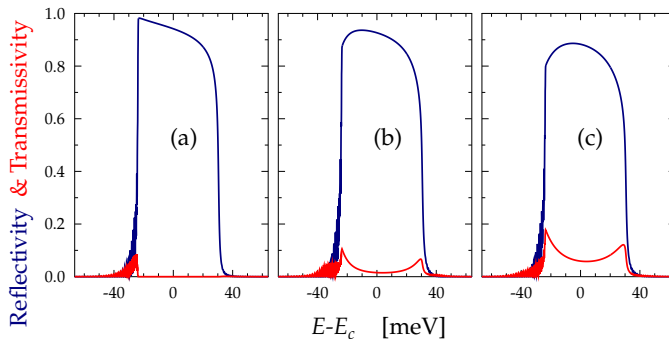


FIG. 2: Spectral reflection profiles (blue) of the four-crystal perfectly aligned *empty* cavity (see Fig. 1) as a result of four successive (400) Bragg reflections of x-rays from diamond crystals B $\rightarrow$ C $\rightarrow$ D $\rightarrow$ A. The transmission profile through crystal A is shown in red. Crystals B, C, and D have a thickness of 300  $\mu\text{m}$ , while crystal A's thickness is (a) 300  $\mu\text{m}$ , (b) 20  $\mu\text{m}$ , and (c) 15  $\mu\text{m}$ , respectively. Photon energy  $E_c = 6.9558$  keV, angular spread (FWHM) of x-rays - 2.5  $\mu\text{rad}$ , Bragg's angle  $\theta = 88^\circ$  ( $\Theta = 2^\circ$ ). The spectral reflection width  $\Delta E_{4 \times (400)} \simeq 54$  meV.

## II. PERMEABLE CRYSTAL OUTPUT COUPLING

The required for the XFEL cavity crystals with close to 100% Bragg reflectivity of x-rays (98%-99.5%) can be achieved only if x-ray transparent crystals are used, for which the ratio of the extinction length  $\bar{\Lambda}_H$  to the photo-absorption length  $L_a$  is very small,  $\bar{\Lambda}_H/L_a \simeq 1/100$ , as in diamond [9]. The extinction length<sup>1</sup>

$$\bar{\Lambda}_H = \frac{\sqrt{\gamma_0 |\gamma_H|}}{\sin \theta} \bar{\Lambda}_H^{(s)}, \quad (1)$$

$$\gamma_0 = \sin(\theta + \eta), \quad \gamma_H = \sin(\eta - \theta) \quad (2)$$

is a measure of penetration of x-rays into the crystal in Bragg diffraction with diffraction vector  $\mathbf{H}$ . Here,  $\theta$  is the glancing angle of incidence to the reflecting atomic planes (Bragg's angle),  $\eta$  is the asymmetry angle between the crystal entrance surface and the reflecting atomic planes, and  $\bar{\Lambda}_H^{(s)}$  is the extinction length in the symmetric scattering geometry, when  $\eta = 0$ .  $\bar{\Lambda}_H^{(s)}$  is to a good accuracy a Bragg reflection invariant in low-absorbing crystals like diamond. The  $\bar{\Lambda}_H^{(s)}$  values for the allowed Bragg reflections in diamond can be found tabulated in [15].

Reflectivity  $R(0)$  and transmissivity  $T(0)$  of a thick ( $d > \bar{\Lambda}_H$ ) x-ray-transparent (low-absorbing) crystal at the center of the Bragg reflection region are

$$R(0) \simeq 1 - 4 \exp(-d/\bar{\Lambda}_H), \quad (3)$$

$$T(0) \simeq 4 \exp(-d/\bar{\Lambda}_H - d/L_a \gamma_0), \quad (4)$$

see, for example Eq.(7.11) of [16]. Therefore, in addition to x-ray transparency, the high reflectivity requires that the crystal thickness is  $d \gtrsim 10\bar{\Lambda}_H$  [17].

To ensure low losses in the cavity, almost all crystals should have a very high reflectivity and therefore should be sufficiently thick. These are crystals B, C, and D in the example shown in Fig. 1. The crystals are in symmetric scattering geometry ( $\eta = 0$ ) to avoid angular dispersion [17, 18], which can deteriorate the transverse profile of the beam.<sup>2</sup> However, one crystal may have reduced reflectivity and therefore some transmissivity to allow for a certain portion of the intracavity beam to be coupled out of the cavity.

Because  $\bar{\Lambda}_H/L_a \ll 1$ , to ensure, say, approximately a 5% transmission, the crystal thickness should be reduced to  $\simeq 4.4\bar{\Lambda}_H$ . Typically  $\bar{\Lambda}_H \simeq 4 - 10$   $\mu\text{m}$  for Bragg reflections in diamond crystals used to backreflect photons with energies in the 7–10-keV range [15]. Therefore, the thickness of a diamond crystal with the 5%-outcoupling efficiency should be about 15–45  $\mu\text{m}$ .

Figure 2 shows examples of spectral Bragg reflection profiles (blue lines) upon successive Bragg reflections from diamond crystals in the four-crystal cavity with the crystals set into the  $\mathbf{H}=(4\ 0\ 0)$  Bragg reflection. The transmission spectra through thin crystal A are shown in red. The profiles were calculated by using the dynamical theory of x-ray Bragg diffraction with crystals B, C, and D being 300  $\mu\text{m}$  thick, and output coupler crystal A being 300  $\mu\text{m}$  (a), 20  $\mu\text{m}$  (b), 15  $\mu\text{m}$  (c). In the latter case the outcoupling efficiency is close to about 5%, and the ratio of the crystal thickness  $d = 15$   $\mu\text{m}$  to the extinction length  $\bar{\Lambda}_{511} = 3.6$   $\mu\text{m}$  is  $d/\bar{\Lambda}_{511} \simeq 4.2$ . Such thin diamond crystals can be manufactured and handled without degrading Bragg diffraction performance [20]. However, extracting more power from the cavity would require much thinner crystals, which are both very difficult to manufacture without introducing crystal defects and very difficult to handle without degrading Bragg diffraction performance.

An even bigger challenge occurs if Bragg reflections with the smallest diffraction vectors  $\mathbf{H}$  for which  $\bar{\Lambda}_H \simeq 1-2$   $\mu\text{m}$  have to be used to backreflect x-ray photons with energies below 5 keV. In all of these cases the thickness required even for the 5%-outcoupling efficiency crystal becomes extremely small,  $d \simeq 4.4\bar{\Lambda}_H \simeq 5 - 10$   $\mu\text{m}$ .

Altogether, outcoupling through a permeable thin crystal is typically limited to a less than  $\simeq 5\%$  efficiency, unless high-indexed Bragg reflections with  $\bar{\Lambda}_H \gtrsim 15$   $\mu\text{m}$  are used that are appropriate for handling x-rays with photon energies  $E \gtrsim 15$  keV.

<sup>1</sup> Here we are using the extinction length as defined in [15]. In other texts, e.g. in [16] an alternative definition is used  $\Lambda_H = 2\pi \bar{\Lambda}_H$ .

<sup>2</sup> A lateral shift of  $\simeq \bar{\Lambda}_H \cos \theta$  of x-rays also takes place in the symmetric scattering geometry [15, 19].

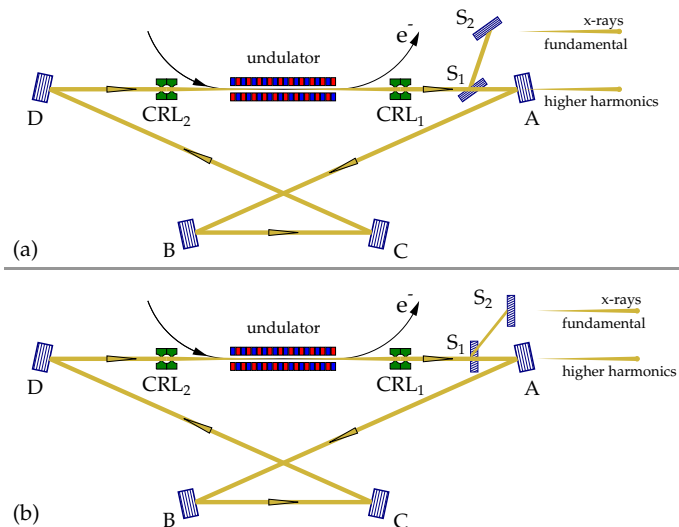


FIG. 3: “Beam-splitter” output coupling methods presented in the example of the four-crystal cavity. In contrast to the scheme of Fig. 1, all four Bragg-reflecting crystals (A, B, C, and D) are thick and are featuring highest reflectivity for the fundamental harmonic. The fundamental is now coupled out through a thin beam-splitter crystal  $S_1$ , while higher harmonics can be coupled out through transparent-for-them crystal A. Beam-splitter crystal  $S_1$  (output coupler) and crystal  $S_2$  designed for fixed-exit outcoupling can be either in the reflection (Bragg-case) geometry (a) or in transmission (Laue-case) geometry (b). Other types of beam splitters can be used instead of the Bragg-reflecting crystals as well.

### III. BEAM-SPLITTER OUTPUT COUPLING

Here we present an alternative method of extracting intracavity radiation power from XFEL cavities, which may have a much higher than 5% efficiency, and in particular may be appropriate for XRAFEL optical cavities. Again, we use the four-crystal cavity as an example, although the technique is applicable to other cavity types as well.

In this approach, all crystals including A are thick ( $d \gtrsim 10\bar{\Lambda}_H$ ) and are featuring high-reflectivity for the fundamental harmonic; see cavity schematics in Fig. 3. The fundamental is outcoupled through an additional beam-splitter crystal  $S_1$  inserted into the intracavity beam and set into Bragg diffraction either in the reflection (Bragg-case) scattering geometry as in Fig. 3(a), or in the transmission (Laue-case) scattering geometry as in Fig. 3(b). The higher harmonics can be still outcoupled through crystal A, whose thickness could be tailored to be transparent for them. To minimize losses in the cavity, the thickness of the beam-splitter crystal should be chosen to be much smaller than the absorption length. This requirement is, however, much less demanding than the a-few-extinction-lengths requirement for the output coupler crystal in the “permeable crystal” method discussed in Sec. II. The amount of outcoupled intracavity power is changed by varying the crystal reflectivity, which can

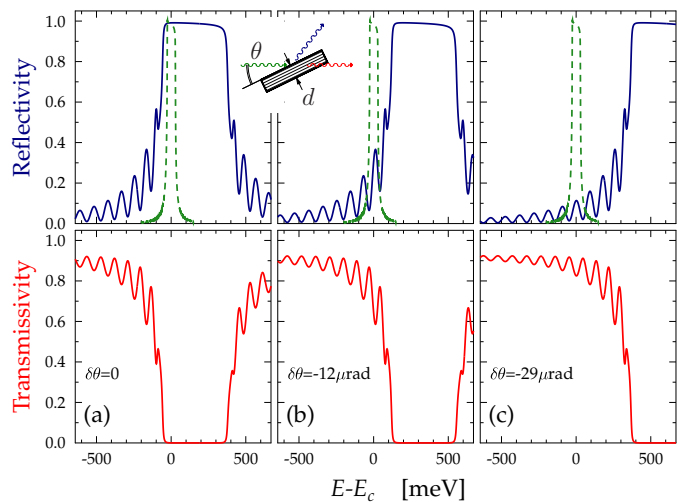


FIG. 4: Reflection (blue) and transmission (red) spectral profiles of x-rays from a  $d = 15\text{-}\mu\text{m}$ -thick diamond beam-splitter crystal  $S_1$  in the symmetric (111) Bragg diffraction ( $\eta = 0$ ). The x-rays are at the incidence angle  $\theta = \bar{\theta} + \delta\theta$  ( $\bar{\theta} = 25.6434^\circ$ ) to the diffraction planes (111): (a)  $\delta\theta = 0$ ; (b)  $\delta\theta = -12\ \mu\text{rad}$ ; (c)  $\delta\theta = -29\ \mu\text{rad}$ . The green dashed line is a reference spectral Bragg reflection profile from  $300\text{-}\mu\text{m}$ -thick diamond crystals in the cavity (as in Fig. 3) which are set to the (400) reflection with Bragg’s angle  $88^\circ$  and centered at  $E_c = 6.9558\ \text{keV}$ .

be achieved either by changing crystal angle or crystal thickness, as discussed below.

There is a second crystal  $S_2$  with the identical Bragg reflection in the non-dispersive (+−) setting, which is used to direct the out-coupled radiation parallel to the undulator axis independent of the photon energy. Use of two additional crystals, with all four in the (+ − − +) configuration, could be also considered to return the x-ray beam to the undulator axis.

Diamond crystals as the beam splitters would be the preferred choice, because of their high x-ray transparency, resilience to radiation and heat load, and high Bragg reflectivity. In fact, diamond crystals have been in use for a long time as Bragg-reflecting beam splitters for multiplexing x-ray beams at storage ring [21, 22] and XFEL [23–25] facilities. In those applications, they are used to extract a narrowband component from the primary broadband beam. In the present case, the task is to extract a certain amount of the intracavity power without changing its spectral composition.

#### A. Bragg-case beam splitter

We consider first the Bragg-case beam splitter as in Fig. 3(a), and assume in all following examples (unless specified otherwise) that the cavity crystals are set into the (400) Bragg reflection with the Bragg angle of  $88^\circ$ . This sets the center of the Bragg reflection range at  $E_c = 6.9558\ \text{keV}$ .

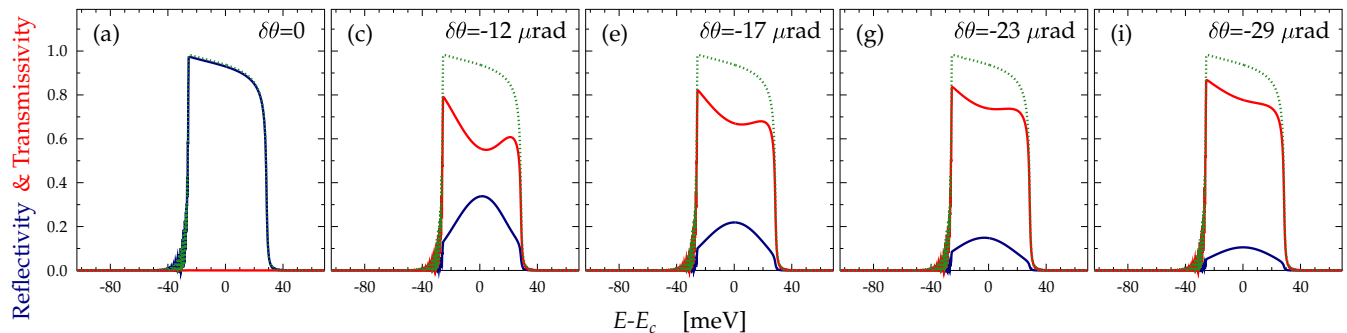


FIG. 5: Spectral profiles: (dotted green) of the radiation in the diamond four-crystal cavity upon successive (400) Bragg reflection from 300- $\mu\text{m}$ -thick diamond crystals A $\rightarrow$ B $\rightarrow$ C $\rightarrow$ D with the central cavity energy  $E_c = 6.9558$  keV; (blue) of the radiation coupled out of the cavity with a beam-splitter crystal in the Bragg-case geometry; (red) of the radiation transmitted through the beam splitter and left in the cavity. The beam splitter is a 15- $\mu\text{m}$ -thick diamond crystal set in the (111) Bragg reflection at incidence angles  $\theta = \bar{\theta} + \delta\theta$  ( $\bar{\theta} = 25.6434^\circ$ ) as in Fig. 4.

The spectral Bragg reflection profile from a thick crystal ( $d \gg \bar{\Lambda}_H$ ) in the reflection (Bragg-case) scattering geometry features close to a 100% reflectivity in a spectral range  $\Delta E_H = E (d_H/\pi\bar{\Lambda}_H)$  around the photon energy  $E = hc/\lambda$  defined by Bragg's law  $\lambda = 2d_H \sin \theta$ . Here,  $d_H$  is the interplanar distance of the reflecting atomic planes corresponding to the diffraction vector  $\mathbf{H}$ , and  $\theta$  is the glancing angle of incidence to the reflecting atomic planes (Bragg's angle). Figure 4(a) shows an example of the Bragg reflection profile (solid blue line) from diamond in the (111) reflection. The initial Bragg angle  $\theta = 25.6434^\circ$  is chosen such that the high-reflectivity range overlaps with the cavity spectral profile (shown by dashed green line) centered at  $E_c = 6.9558$  keV. The solid red line in the bottom graph shows the corresponding spectral transmission dependence. The (111) Bragg reflection parameters are:  $d_{111} = 2.059$  Å,  $\bar{\Lambda}_{111} = 1.1$   $\mu\text{m}$ , and  $\Delta E_{111} = 520$  meV.

Intensity oscillations – equal thickness fringes – are observed on the tails of the reflection dependence. The period of the oscillations is

$$\delta E = \frac{hc}{2d} \frac{\gamma_H}{\sin^2 \theta} \quad \text{or} \quad \delta E = \frac{hc}{2d \sin \theta} \quad \text{if } \eta = 0, \quad (5)$$

see Eq. (2.176) of [17]. In the example shown in Fig. 4,  $\delta E = 95$  meV for a  $d=15$ - $\mu\text{m}$ -thick crystal at  $\theta = 25.64^\circ$ .

For a much thicker crystal, the period becomes very small and the oscillations wash out, as illustrated by the dashed green line in Fig. 4 calculated for  $d=300$ - $\mu\text{m}$ -thick cavity crystals A, B, C, and D in the (400) Bragg reflection with a spectral width of  $\Delta E_{400} = 54$  meV.

If the period of oscillations is tailored to be larger than the cavity bandwidth, the fringes can be tuned to the center  $E_c$  of the cavity band with a purpose of outcoupling a desired amount of the intracavity power. The tuning is achieved by varying the glancing angle of incidence  $\theta$  of x-rays to the reflecting atomic planes. In the example shown in Fig. 5,  $\delta E = 95$  meV, while the cavity bandwidth  $\Delta E_{400} = 54$  meV. The amount of the intracavity power, which can be outcoupled, changes from almost

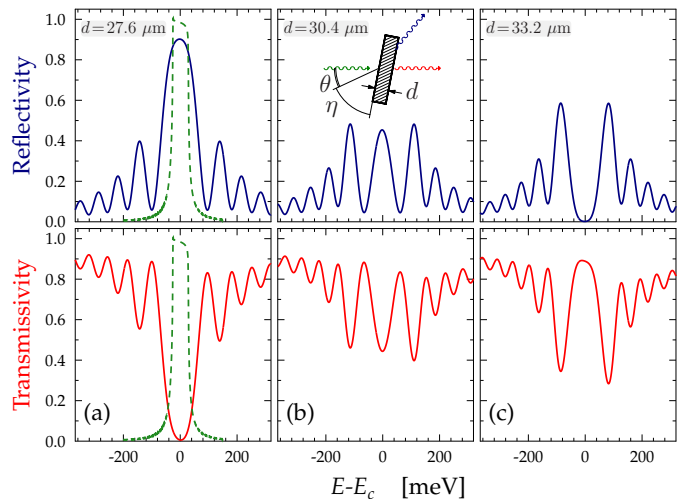


FIG. 6: Reflection (blue) and transmission (red) spectral profiles of x-rays in a diamond beam-splitter crystal  $S_1$  set to the (111) Bragg diffraction in Laue-case geometry with  $\eta = 54.74^\circ$  [the entrance crystal surface is parallel to the (100) planes]. The profiles are calculated for the crystal thickness  $d$  varying with an increment of  $\bar{\Lambda}_H/4$  of the Pendelösung period  $\bar{\Lambda}_H = 11$   $\mu\text{m}$ : (a)  $d = 27.6$   $\mu\text{m}$ ; (b)  $d = 30.4$   $\mu\text{m}$ ; and (c)  $d = 33.2$   $\mu\text{m}$ . The spectral profiles and the cavity reflection profile (dashed green lines) are centered at the same energy  $E_c = 6.9558$  keV. The x-rays are at the incidence angle  $\theta = 25.6434^\circ$  to the diffraction planes (111) and at  $88^\circ$  to the (400) planes in the cavity crystals.

zero to  $\simeq 30$ -40%, i.e., much larger than what the permeable thin-crystal outcoupling technique can realistically provide.

## B. Laue-case beam splitter

Even larger outcoupling efficiency can be achieved with the Bragg-diffracting beam-splitter crystal in the trans-



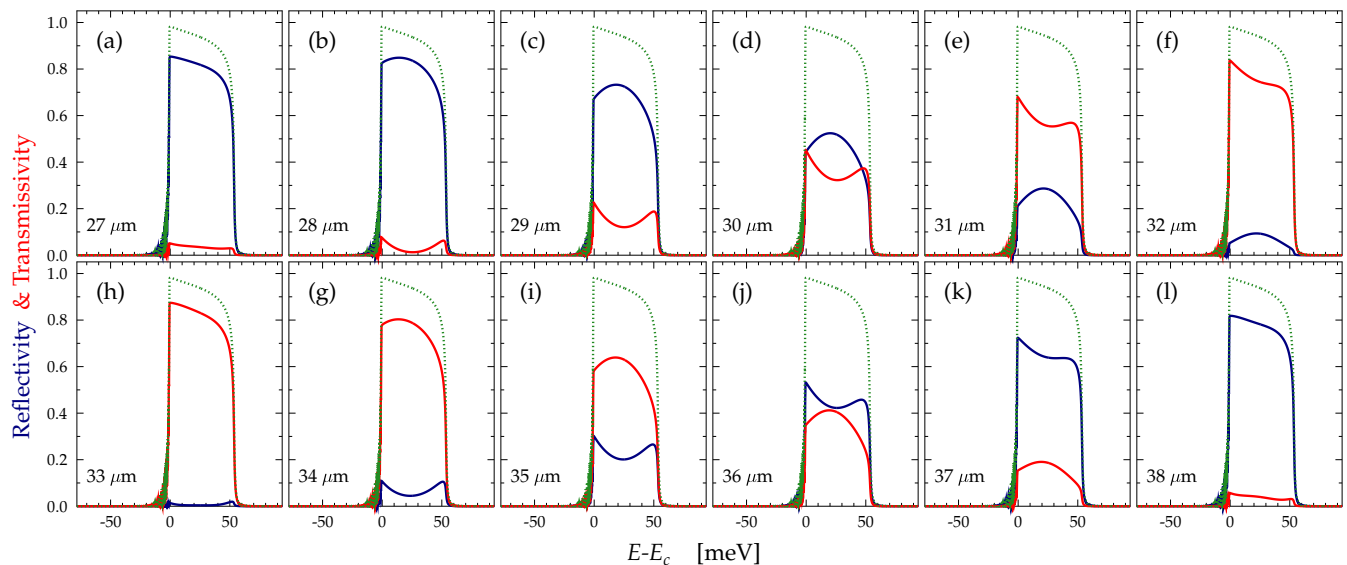


FIG. 7: Similar to Fig. 5; however, the beam-splitter crystal is in the transmission (Laue-case) geometry; see Fig. 3(b). The beam-splitter crystal thickness  $d$  varies from  $27 \mu\text{m}$  (a) to  $38 \mu\text{m}$  (l). Other parameters are provided in the caption to Fig. 6. Instead of varying the crystal thickness, azimuthal angle  $\phi$  can be varied alternatively by crystal rotation about the diffraction vector in the range from about  $0$  to  $35^\circ$ .

mission (Laue-case) scattering geometry as in Fig. 3(b). This is possible due to the Pendellösung effect [26], a unique feature for this scattering geometry; see also [16]. In the Laue-case scattering geometry, both the Bragg-diffracted (BD) and forward-Bragg-diffracted (FBD) beams are on the same side of the crystal. There is a periodic exchange of energy between the two beams, propagating through the crystal thickness, as between two coupled pendulums. When one is in maximum, another is in minimum and vice versa. As a result, the BD and FBD intensities are complementary oscillating functions of the crystal thickness, the Pendellösung effect, which is illustrated in Figs. 6(a)-(c) on the example of the spectral profiles calculated for three different crystal thicknesses  $d$  at a fixed glancing angle of incidence  $\theta$ . There is almost zero transmission and  $\simeq 90\%$  reflectivity at  $E = E_c$  in Fig. 6(a), while the picture reverses in Fig. 6(c). The Pendellösung period is equal to  $\Lambda_H = 2\pi\bar{\Lambda}_H$ , where  $\bar{\Lambda}_H$  is the extinction length given by Eq. (1). In particular, for the case of the beam-splitter crystal presented in Fig. 6,  $\bar{\Lambda}_{111}^{(s)} = 1.1 \mu\text{m}$ ,  $\bar{\Lambda}_{111} = 1.75 \mu\text{m}$ , and  $\Lambda_{111} = 11 \mu\text{m}$ .

Furthermore, the BD and FBD intensities are also complementary oscillating functions of the photon energy, featuring the equal thickness fringes as in the Bragg-case geometry; see Fig. 4.

The width of the central maxim (minimum) at  $E = E_c$  in the Laue-case diffraction is roughly about two periods of the equal thickness fringes, given by Eq. (5), and amounts to  $\simeq 120 \text{ meV}$  in the present case. Because the width is much larger than the  $54\text{-meV}$  bandwidth of the cavity, this beam splitter can outcouple efficiently the intracavity power, as the results of calculations show in Fig. 7. When the crystal thickness is  $d = 2.5\Lambda_H \simeq 27 \mu\text{m}$ ,

the maximum reflectivity is achieved and almost 90% of the intracavity power is outcoupled; see Fig. 7(a). If  $d = 3\Lambda_H \simeq 33 \mu\text{m}$ , the reflectivity is lowest and the transmissivity is highest, as in Fig. 7(h). Figures 7(h)-(l) show the reverse process. Crystal thickness variation can be accomplished, for example, if the crystal has a wedge form. Alternatively, instead of physically changing the crystal thickness in this range, the azimuthal angle can be varied in the range from about  $0$  to  $35^\circ$  by rotating the crystal around the  $(111)$  diffraction vector.

If the width of the equal thickness fringes are broader or equal to the cavity bandwidth, outcoupling can also be achieved by tuning the fringes to the cavity bandwidth center by properly selecting the glancing angle of incidence  $\theta$ , as the results of calculations show in Fig. 8. Varying the outcoupling efficiency by changing the angle is straightforward; however, with this approach it is difficult to reach the 90% outcoupling efficiency possible by crystal thickness variation and the Pendellösung effect, as in Fig. 7. These results are similar to outcoupling using equal thickness fringes in the Bragg-case geometry presented in Fig. 5; however, in the Laue-case, the crystal thickness can be several times larger, which is an advantage.

Altogether, outcoupling with the beam splitter in the Laue-case geometry seems to be preferred compared to the beam-splitter case in the Bragg-case geometry. However, there is a complication in the Laue-case, which has to be handled appropriately. If the asymmetry angle  $\eta$  is nonzero, as in the Laue-case geometry (see Fig. 6) angular dispersion takes place, resulting in detrimental distortions of the wavefront and coherence; see, for example, [15, 17, 27, 28]. To undo this effect, Bragg diffraction

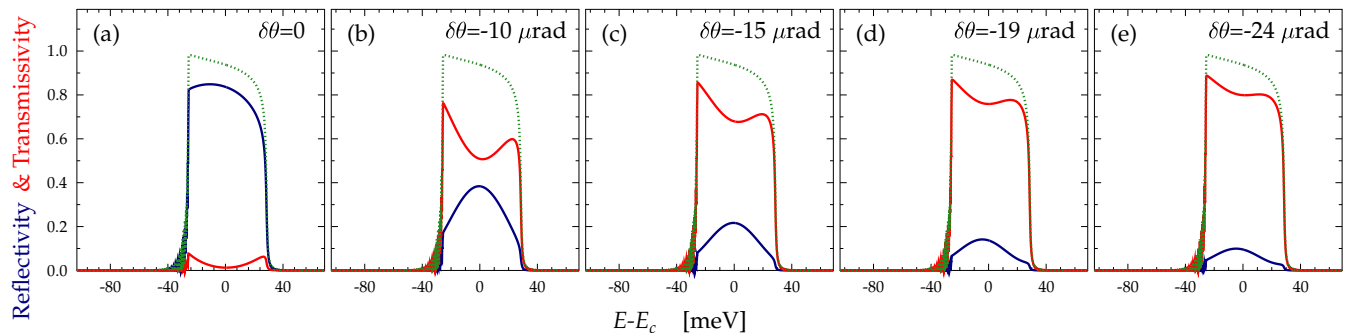


FIG. 8: Similar to Fig. 7, however the beam splitter shown in Fig. 3(b) is a diamond crystal with a fixed  $28\text{-}\mu\text{m}$  thickness set in the (111) Bragg reflection at incidence angles  $\theta = \tilde{\theta} + \delta\theta$  ( $\tilde{\theta} = 25.6434^\circ$ ) as in Fig. 6(a).

from the second crystal  $S_2$  can be applied identical to  $S_1$ , as in Fig. 3(b); however, in a time-reversed setting with the asymmetry angle  $\pi - \eta$ , where  $\eta$  is the asymmetry angle of the first crystal. Crystal  $S_2$  should have a thickness of  $(n + 1/2)\Lambda_H$ , where  $n = 0, 1, 2, \dots$  ensuring the highest reflectivity in Laue-case geometry.

#### IV. DISCUSSION

In the present paper we consider different approaches for coupling x-rays out of XFEL cavities. A standard approach of using permeable thin-crystal Bragg reflecting mirrors is very often limited to extraction only a few percentage points of the intracavity's power. This is acceptable for low-gain XFEL oscillators. The high-gain regenerative amplifier XFEL requires, however, much higher outcoupling efficiency. Using Bragg reflecting pinhole crystal mirrors for this purpose is a possibility discussed in [14]. Here we analyze an alternative approach: intracavity Bragg-reflecting crystal beam splitters.

There are significant advantages in this approach. First, the out-coupled power can be varied over a large range, from almost zero to nearly 100%, by varying the crystal thickness or orientation. Second, extremely thin crystals are not required. The crystals have only to be much thinner than the absorption length in diamond.

Third, fundamental and higher harmonics can be out-coupled at different locations. Fourth, multi-beam out-coupling to increase the number of users can be achieved by installing additional beam-splitter crystal pairs  $S_1$ - $S_2$  at different locations in the cavity.

Other types of beam splitters can be used as well. Grazing incidence mirrors or crystals in Bragg diffraction with sharp edges can be used as wavefront-division beam splitters [29]. X-ray transparent diamond diffraction gratings also can be considered [30–32]. However, there are always two beams in each diffraction order, and several diffraction orders can contribute. Many beams could be good or bad depending on the application.

#### V. ACKNOWLEDGMENTS

Kwang-Je Kim (Argonne National Laboratory) is acknowledged for the discussion of importance of efficient outcoupling schemes. Anne Sakdinawat, David Attwood, and Diling Zhu (SLAC National Laboratory) are acknowledged for sharing results on hard-x-ray high-fidelity diamond-grating beam splitters. Work at Argonne National Laboratory was supported by the U.S. Department of Energy, Office of Science, Office of Basic Energy Sciences, under contract DE-AC02-06CH11357.

- 
- [1] A. M. Kondratenko and E. L. Saldin, *Part. Accel.* **10**, 207 (1980).
  - [2] R. Bonifacio, C. Pellegrini, and L. Narducci, *Opt. Commun.* **50**, 373378 (1984).
  - [3] P. Emma, R. Akre, J. Arthur, R. Bionta, C. Bostedt, J. Bozek, A. Brachmann, P. Bucksbaum, R. Coffee, F.-J. Decker, et al., *Nature Photonics* **4**, 641 (2010).
  - [4] Z. Huang and R. D. Ruth, *Phys. Rev. Lett.* **96**, 144801 (2006).
  - [5] K.-J. Kim, Yu. Shvyd'ko, and S. Reiche, *Phys. Rev. Lett.* **100**, 244802 (2008).
  - [6] K.-J. Kim and Yu. V. Shvyd'ko, *Phys. Rev. ST Accel. Beams* **12**, 030703 (2009).
  - [7] R. R. Lindberg, K.-J. Kim, Yu. Shvyd'ko, and W. M. Fawley, *Phys. Rev. ST Accel. Beams* **14**, 010701 (2011).
  - [8] Yu. Shvyd'ko, *Beam Dynamics Newsletter* **60**, 68 (2013), International Committee for Future Accelerators.
  - [9] Yu. V. Shvyd'ko, S. Stoupin, V. Blank, and S. Terentyev, *Nature Photonics* **5**, 539 (2011).
  - [10] B. Lengeler, C. Schroer, J. Tümmler, B. Benner, M. Richwin, A. Snigirev, I. Snigireva, and M. Drakopoulos, *J. Synchrotron Radiation* **6**, 1153 (1999).
  - [11] T. Kolodziej, S. Stoupin, W. Grizolli, J. Krzywinski, X. Shi, K.-J. Kim, J. Qian, L. Assoufid, and

- Yu. Shvyd'ko, *Journal of Synchrotron Radiation* **25**, 354 (2018).
- [12] D. C. Nguyen, R. L. Sheffield, C. M. Fortgang, J. C. Goldstein, J. M. Kinross-Wright, and N. A. Ebrahim, *Nuclear Instruments and Methods in Physics Research Section A: Accelerators, Spectrometers, Detectors and Associated Equipment* **429**, 125 (1999), ISSN 0168-9002.
- [13] G. Marcus, Y. Ding, J. Duris, Y. Feng, Z. Huang, J. Krzywinski, T. R. T. Maxwell, K.-J. Kim, R. Lindberg, Yu. Shvyd'ko, et al., in *Proceedings of 38th International Free Electron Laser Conference* (Santa Fe, NM, USA, 2017).
- [14] H. Freund, P. van der Slot, and Yu. Shvyd'ko, arXiv:1905.06279 (2019).
- [15] Yu. Shvyd'ko and R. Lindberg, *Phys. Rev. ST Accel. Beams* **15**, 100702 (2012).
- [16] A. Authier, *Dynamical Theory of X-Ray Diffraction*, vol. 11 of *IUCr Monographs on Crystallography* (Oxford University Press, Oxford, New York, 2001).
- [17] Yu. Shvyd'ko, *X-Ray Optics – High-Energy-Resolution Applications*, vol. 98 of *Optical Sciences* (Springer, Berlin, 2004).
- [18] Yu. V. Shvyd'ko, M. Lerche, U. Kuetgens, H. D. Rüter, A. Alatas, and J. Zhao, *Phys. Rev. Lett.* **97**, 235502 (2006).
- [19] R. R. Lindberg and Yu. V. Shvyd'ko, *Phys. Rev. ST Accel. Beams* **15**, 050706 (2012).
- [20] T. Kolodziej, P. Vodnala, S. Terentyev, V. Blank, and Yu. Shvyd'ko, *Journal of Applied Crystallography* **49**, 1240 (2016).
- [21] J. Als-Nielsen, A. Freund, G. Grübel, J. Linderholm, M. Nielsen, M. del Rio, and J. Sellschop, *Nucl. Instrum. Methods Phys. Res. B* **94**, 306 (1994).
- [22] M. Mattenet, T. Schneider, and G. Grübel, *Journal of Synchrotron Radiation* **5**, 651 (1998).
- [23] D. Zhu, Y. Feng, S. Stoupin, S. A. Terentyev, H. T. Lemke, D. M. Fritz, M. Chollet, J. M. Glowina, R. Alonso-Mori, M. Sikorski, et al., *Rev. Sci. Instrum.* **85**, 063106 (2014).
- [24] S. Stoupin, S. A. Terentyev, V. D. Blank, Yu. V. Shvyd'ko, K. Goetze, L. Assoufid, S. N. Polyakov, M. S. Kuznetsov, N. V. Kornilov, J. Katsoudas, et al., *Journal of Applied Crystallography* **47**, 1329 (2014).
- [25] Y. Feng, R. Alonso-Mori, T. R. M. Barends, V. D. Blank, S. Botha, M. Chollet, D. S. Damiani, R. B. Doak, J. M. Glowina, J. M. Koglin, et al., *Journal of Synchrotron Radiation* **22**, 626 (2015).
- [26] P. P. Ewald, *Ann. Physik* **54**, 519 (1917).
- [27] S. Brauer, G. Stephenson, and M. Sutton, *J. Synchrotron Radiation* **2**, 163 (1995).
- [28] A. Souvorov, M. Drakopoulos, I. Snigireva, and A. Snigirev, *J. Phys. D: Appl. Phys.* **32**, A184 (1999).
- [29] T. Hirano, T. Osaka, Y. Morioka, Y. Sano, Y. Inubushi, T. Togashi, I. Inoue, S. Matsuyama, K. Tono, A. Robert, et al., *Journal of Synchrotron Radiation* **25**, 20 (2018).
- [30] P. Karvinen, S. Rutishauser, A. Mozzanica, D. Greiffenberg, P. Juranic, A. Menzel, A. Lutman, J. Krzywinski, D. Fritz, H. Lemke, et al., *Optics Letters* **37**, 5073 (2012).
- [31] M. Makita, P. Karvinen, D. Zhu, P. N. Juranic, J. Grnert, S. Cartier, J. H. Jungmann-Smith, H. T. Lemke, A. Mozzanica, S. Nelson, et al., *Optica* **2**, 912 (2015).
- [32] K. Li, A. Sakdinawat, and et al., t.b.p. (2019).